Peishan Li, Yu Song, Wenying Zan, Liping Qin, Shuang Han, Baichun Jiang, Hao Dou, Changshun Shao, and Yaoqin Gong

Lack of CUL4B in Adipocytes Promotes PPARγ-Mediated Adipose Tissue Expansion and Insulin Sensitivity

Diabetes 2017;66:300–313 | DOI: 10.2337/db16-0743

Obesity and obesity-associated diseases are linked to dysregulation of the peroxisome proliferator–activated receptor γ (PPARγ) signaling pathway. Identification of the factors that regulate PPARγ expression and activity is crucial for combating obesity. However, the ubiquitin E3 ligases that target PPARγ for proteasomal degradation have been rarely identified, and their functions in vivo have not been characterized. Here we report that CUL4B-RING E3 ligase (CRL4B) negatively regulates PPARγ by promoting its polyubiquitination and proteasomal degradation. Depletion of CUL4B led to upregulation of PPARγ-regulated genes and facilitated adipogenesis. Adipocyte-specific *Cul4b* knockout (AKO) mice being fed a high-fat diet exhibited increased body fat accumulation that was mediated by increased adipogenesis. However, AKO mice showed improved metabolic phenotypes, including increased insulin sensitivity and glucose tolerance. Correspondingly, there was a decreased inflammatory response in adipose tissues of AKO mice. Genetic inhibition of CUL4B thus appears to phenocopy the beneficial effects of PPARγ agonists. Collectively, this study establishes a critical role of CRL4B in the regulation of PPARγ stability and insulin sensitivity and suggests that CUL4B could be a potential therapeutic target for combating obesity and metabolic syndromes.

Peroxisome proliferator–activated receptor γ (PPARγ) is a ligand-dependent nuclear receptor highly expressed in adipose tissue. PPARγ has been demonstrated to be a necessary and sufficient regulator of adipogenesis and has also been shown to control glucose homeostasis and insulin sensitivity (1–3). Dysregulation of PPARγ leads to obesity and obesity-associated diseases. Consequently, PPARγ agonists such as thiazolidinediones (TZDs) are widely used in the treatment of type 2 diabetes (4,5). However, TZDs have severe side effects such as weight gain, fluid retention, and cardiovascular dysfunctions (6,7). Therefore, elucidation of the factors that regulate PPARγ expression and activity will further our understanding of adipocyte biology and help to develop better therapeutic interventions.

PPARγ expression and activity are regulated at different levels from transcription to post-translational modification (8,9). Recent studies (10–14) suggest that covalent modifications of PPARγ, including phosphorylation, ubiquitination, and SUMOylation, affect the protein stability and transcriptional activity of PPARγ. PPARγ proteins have a short half-life in adipocytes, and their turnover is regulated by the ubiquitin (Ub)-proteasome system (15,16). However, the E3 ligases that target PPARγ for proteasomal degradation rarely have been identified, and their functions in vivo have not been characterized.

CUL4B-RING E3 ligases (CRL4Bs) have been shown to participate in the regulation of diverse physiologically and developmentally controlled processes by targeting different substrates for Ub-dependent degradation or modification (17–19). Mutations in human *CUL4B* are a common cause of X-linked mental retardation (20,21). In addition to being mentally retarded, patients with *CUL4B* mutations also manifest central obesity, implicating that CUL4B could be involved in obesity and energy homeostasis. Here, we investigated the role of CUL4B in adipogenesis and insulin sensitivity and demonstrated that CUL4B functions as a negative regulator of adipogenesis via targeting PPARγ for proteasomal degradation. Adipocyte-specific

The Key Laboratory of Experimental Teratology, Ministry of Education and Department of Molecular Medicine and Genetics, Shandong University School of Medicine, Jinan, Shandong, People's Republic of China

Corresponding author: Yaoqin Gong, yxg8@sdu.edu.cn.

Received 16 June 2016 and accepted 5 November 2016.

This article contains Supplementary Data online at http://diabetes.diabetesjournals.org/lookup/suppl/doi:10.2337/db16-0743/-/DC1.

Cul4b knockout (AKO) mice exhibited increased adiposity relative to wild-type (WT) control when challenged with a high-fat diet (HFD). However, despite the increased obesity, the AKO mice showed improved metabolic parameters.

RESEARCH DESIGN AND METHODS

Animals

The *Cul4b* floxed mice were generated as reported previously (22). To generate AKO mice (*Fabp4*-cre$^{+/-}$*Cul4b*$^{flox/y}$), *Cul4b*$^{flox/flox}$ mice were crossed to *Fabp4*-cre$^{+/-}$ mice (1). Their age-matched littermates *Fabp4*-cre$^{-/-}$*Cul4b*$^{flox/y}$ mice were used as controls (WT). Starting at 8 weeks of age, mice were fed an HFD (D12492; Research Diets) consisting of 60% fat or a normal chow diet (NCD). For PPARγ inhibitor GW9662 treatment, grouped 8-week-old mice were given the HFD for 16 weeks. During the 8–16 weeks, the mice were administered GW9662 or vehicle (corn oil) (4 mg/kg body wt i.p. injection, three times per week). For the pair-feeding experiment, 8-week-old AKO mice were restricted to the same amount of food as that consumed by WT mice for 10 weeks, and their body weights were monitored weekly. All animal experiments were performed in compliance with national regulations and approved by the Animal Care and Use Committee, Shandong University School of Medicine (No. LL-201202001).

Human Subcutaneous Adipose Tissue

Biopsy samples of subcutaneous adipose tissue were obtained from 25 Chinese women receiving elective surgery in Qilu Hospital of Shandong University. Height (in meters) and weight (in kilograms) were measured to determine the BMI. The age of the subjects ranged from 37 to 60 years, and all subjects had a BMI between 19.63 and 38.06 kg/m^2. The study received ethical clearance from Qilu Hospital of Shandong University, and all subjects provided written informed consent prior to surgery.

Metabolic Studies

Mice were fasted overnight, and tail vein blood was collected. Plasma samples were stored at −20°C until use. Concentrations of insulin and adiponectin were measured using ELISA kits. Concentrations of free fatty acid were measured using an assay kit (Wako Diagnostics). For the glucose tolerance test, mice were fasted overnight and then treated by intraperitoneal injection of 0.75 g/kg glucose, followed by measurement of blood glucose levels with a glucometer. To assess insulin tolerance, mice were fasted for 4 h before receiving an injection of insulin (1.5 units/kg body wt i.p.) and were then subjected to measurement of blood glucose levels.

Histological Analysis

The isolated adipose tissues were fixed in 4% formaldehyde/PBS and maintained at 4°C until use. The fixed tissues were dehydrated and processed for paraffin embedding, and 4-μm sections were cut followed by staining with hematoxylin-eosin or indicated antibodies.

In Vitro Chemotaxis Assay

An in vitro chemotaxis assay was performed as previously described (11). Briefly, 1×10^5 peritoneal macrophages from WT mice were placed in the upper chamber of an 8-μm polycarbonate filter (Corning), and primary adipocyte–conditioned medium was placed in the lower chamber. Cells were fixed and stained with crystal violet after 24 h.

Stromal Vascular Fraction Isolation and FACS Analysis

The stromal vascular fractions (SVFs) were isolated by the method described previously (11). After 15 min of incubation with Fc block, SVFs were resuspended in FACS buffer (1% BSA in PBS) and stained with appropriate antibodies conjugated to fluorochromes or isotype controls for 30 min at 4°C in the dark. Then the samples were run on a FACSCanto II flow cytometer (BD) and analyzed using FlowJo (TreeStar) software.

Glucose Uptake

Glucose uptake was assayed as described previously (23) with slight modifications. Induced 3T3-L1 adipocytes were cultured overnight in serum-free DMEM with GW9662 (1 μmol/L) or DMSO control. Cells were then washed with PBS and incubated in glucose-free Krebs-Ringer bicarbonate HEPES buffer (0.1% fatty acid–free BSA) for 15 min. Subsequently, 0.5 μCi 2-[1, 2-^{3}H(N)]-deoxy-D-glucose (PerkinElmer) and 0.1 mmol/L 2-deoxyglucose were added. After 5 min, the reaction was terminated by washing with ice-cold PBS immediately. Aliquots of cell lysates were used for liquid scintillation and for protein concentration determination. For glucose transport in isolated mouse adipocytes, adipocytes were preincubated in glucose-free Krebs-Ringer bicarbonate HEPES buffer containing insulin (10 nmol/L) for 30 min. Then ^{3}H-glucose was added to incubation for 5 min. Results were normalized for protein concentration.

Ub Ligation Assays

In vitro and in vivo ubiquitination assays were performed as described previously (19). For in vitro ubiquitination assays, His-tagged PPARγ was ectopically expressed in *Escherichia coli*. ProA-tagged CUL4B was immunoprecipitated from HEK293T cells transfected with pCUL4B-tobacco etch virus-ProA. After cleavage with tobacco etch virus protease, purified CRL4B complex was achieved.

Statistical Analyses

All data are presented as the mean ± SEM or the mean ± SD. A two-tailed Student *t* test or ANOVA (Tukey test) was used for comparison between or among experiment groups, with P values <0.05 considered to be significant. The correlation between CUL4B expression and BMI was evaluated by nonparametric Spearman test (GraphPad Software).

RESULTS

CUL4B Negatively Regulates Adipogenesis

We first determined whether the expression level of CUL4B is correlated with adipogenesis. As shown in Supplementary

Fig. 1, CUL4B was detected in white adipose tissue (WAT) including epididymal WAT (epiWAT; visceral) and inguinal WAT (ingWAT; subcutaneous) as well as brown adipose tissue (BAT). Interestingly, when C57BL/6 mice were induced to develop obesity by eating an HFD, CUL4B expression in WAT was significantly downregulated, whereas the expression of its paralog CUL4A remained unaltered (Fig. 1*A*). Similarly, a decrease in CUL4B expression was detected in adipose tissues from leptin receptor mutant (*db/db*) mice, a model of obesity and type 2 diabetes, when compared with adipose tissue from WT mice (Fig. 1*B*). Importantly, the expression levels of CUL4B protein in human subcutaneous adipose tissue were inversely correlated with BMI (Fig. 1*C* and Supplementary Fig. 2). Thus, the expression of CUL4B appears to be negatively correlated with obesity, both in mice and humans.

Immunoblot (IB) analysis of CUL4B revealed that CUL4B was highly expressed in 3T3-L1 preadipocytes but was significantly downregulated during adipocyte differentiation (Fig. 1*D*). To further confirm the role of CUL4B in adipocyte differentiation, 3T3-L1 preadipocytes were infected with lentivirus expressing short hairpin RNA (shRNA) for *Cul4b* or a nontargeting control shRNA, and their ability to undergo differentiation into mature adipocytes under stimulation was evaluated by Oil Red O staining of lipid accumulation. CUL4B knockdown caused a remarkable increase in Oil Red O staining (Fig. 1*E*). Consistently, quantitative RT-PCR revealed that the mRNA levels of adipocyte-specific genes, including *Fabp4*,

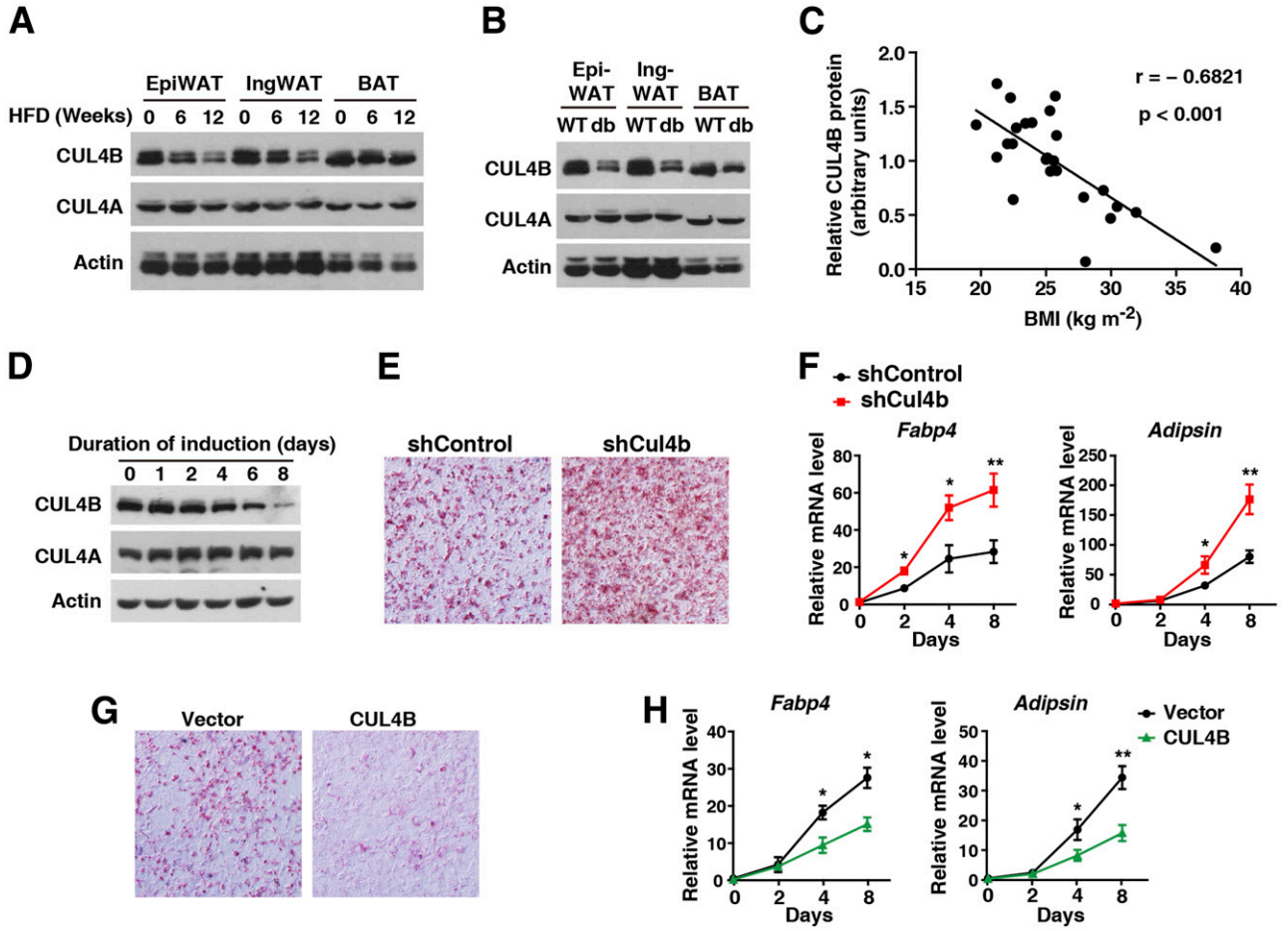

Figure 1—CUL4B negatively regulates adipogenesis. *A*: The 8-week-old male C57BL/6 mice (n = 3 per group) were fed an HFD for an additional 6 or 12 weeks, then the adipose tissue was harvested and immunoblotted with the indicated antibodies. *B*: The indicated protein levels in adipose tissue of 12-week-old WT and *db/db* mice (n = 4 per group). *C*: Negative correlation of CUL4B protein levels in human subcutaneous adipose tissue with BMI. Protein levels were expressed as the band intensity after normalization to loading control, and correlation was assessed by nonparametric Spearman test. *D*: 3T3-L1 cells were differentiated with induced medium, and then the cell lysates were subjected to IB. *E* and *F*: 3T3-L1 stable cell lines were constructed using a lentivirus-expressing shRNA for scrambled sequences (control) or mouse *Cul4b*. *E*: On day 8 after the induction of differentiation, cells were stained with Oil Red O. *F*: At different time points after treatment, total RNA samples were extracted and subjected to quantitative PCR analysis of adipogenic markers (*Fabp4*, *Adipsin*). *G* and *H*: 3T3-L1 cells stably expressing empty vector or CUL4B were constructed using a lentivirus system. *G*: At day 8 post-induction, the cells were stained for lipid droplets with Oil Red O. *H*: The mRNA levels were analyzed by quantitative PCR. Duration of induction is reported in days. The data are presented as the mean ± SD. **P* < 0.05, ***P* < 0.01 by Student *t* test.

Adipsin, *Cd36*, *Lpl*, *Glut4*, and *Adiponectin*, were significantly enhanced. However, the genes responsible for lipolysis and lipid oxidation were largely unchanged (Fig. 1*F* and Supplementary Fig. 3*A* and *B*). In contrast, the overexpression of CUL4B led to decreased lipid accumulation and markedly impaired the induction of adipocyte-specific genes (Fig. 1*G* and *H* and Supplementary Fig. 3*C* and *D*). These findings suggest that CUL4B negatively regulates adipogenesis.

Adipocyte-Specific *Cul4b* Knockout Mice Are Predisposed to Obesity

To assess the role of CUL4B in adipogenesis and metabolic homeostasis in vivo, we generated an adipocyte-specific knockout mouse line (referred to as AKO) on a C57BL/6 background by crossing $Cul4b^{flox/flox}$ mice, in which exons 3–5 of the *Cul4b* gene are flanked by loxP sites (22), to *Fabp4-Cre* transgenic mice (1). As shown in Fig. 2*A*, CUL4B was effectively ablated in adipose tissues but not in

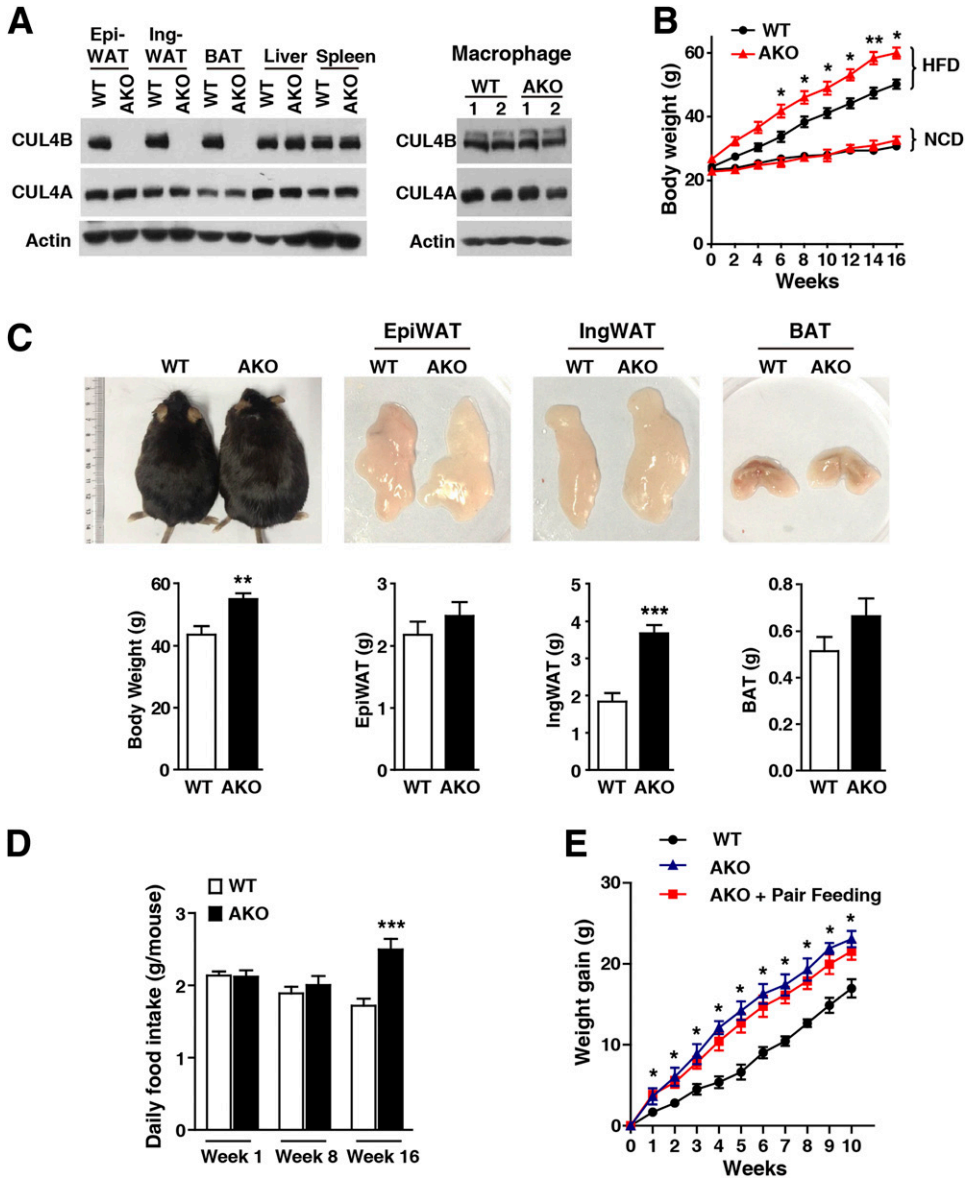

Figure 2—HFD-fed AKO mice are predisposed to obesity. *A*: Left, the protein level in various tissues of WT and AKO mice. Right, the protein level in peritoneal macrophages of WT and AKO mice. *B*: Body weight of WT and AKO mice during 16 weeks of NCD or HFD feeding (n = 7–8 for each group). $^*P < 0.05$, $^{**}P < 0.01$ for HFD-fed WT vs. AKO. *C*: The 8-week-old male WT (n = 7) and AKO (n = 7) mice were fed an HFD for an additional 16 weeks. Representative photographs of mice as well as fat pads (epididymal, inguinal, and BAT) (top). Body and fat pad weights in absolute amounts (bottom). *D*: Daily food intake was monitored during the first, the eighth, and the last week of HFD feeding (n = 7 for each group). *E*: Pair-feeding experiment. The 8-week-old WT and AKO mice were placed on an HFD for an additional 10 weeks. WT, ad libitum–fed WT mice; AKO, ad libitum–fed AKO mice; AKO+Pair feeding, AKO mice fed with the same amount of food as consumed by WT mice, n = 5 for each group. $^*P < 0.05$ for WT vs. AKO+Pair feeding by ANOVA (*E*). All data are presented as the mean ± SEM. $^*P < 0.05$, $^{**}P < 0.01$, $^{***}P < 0.001$, except where otherwise stated, by Student t test.

nonadipose tissues, including peritoneal macrophages, indicative of adipocyte-restricted Cre expression and consistent with previous studies using this *Fabp4-Cre* mouse line (1,11). Furthermore, the deletion of *Cul4b* did not affect the expression of CUL4A (Fig. 2*A*). The AKO mice did not exhibit overt abnormalities. The 8-week-old AKO mice and WT littermates were then fed either a NCD or HFD for 16 weeks. After eating the NCD, AKO mice were undistinguishable in body weight, food intake, and fat mass from WT mice (Fig. 2*B* and Supplementary Fig. 4*A–E*). However, when placed on an HFD, the weight gain in AKO mice was significantly accelerated compared with their WT littermates (Fig. 2*B* and *C*). At 24 weeks of age, ingWAT mass was significantly greater in AKO mice than in WT (3.67 ± 0.60 g vs. 1.84 ± 0.61 g, $P < 0.001$), whereas the masses of epiWAT and BAT in AKO mice were slightly increased (Fig. 2*C*). Because differential food intake or energy expenditure could contribute to enhanced weight gain in HFD-fed AKO mice, we examined food intake and metabolic parameters. As in NCD-fed mice, no difference in 24-h food intake was detected at the starting point. Importantly, there was no significant difference in food intake during the first 8 weeks of HFD feeding, whereas a greater body weight gain in AKO mice was already evident (Fig. 2*D*). However, AKO mice showed increased food intake near the end of the observation period (Fig. 2*D*). To further exclude increased food intake as a contributer to the increased body weight gain in AKO mice, we placed 8-week-old AKO mice on pair feeding for 10 weeks. Although AKO mice were restricted to the same amount of food as that consumed by WT mice, they gained more body weight than WT mice at all time points examined (Fig. 2*E*). Furthermore, the basal circulating leptin level and the response to injected leptin remained the same between AKO and WT littermates (Supplementary Fig. 5*A–C*). These results indicate that the increased predisposition to obesity in AKO mice is unlikely to be caused by increased food intake. Moreover, there was no difference in oxygen consumption, carbon dioxide production, and respiratory exchange ratio as well as in locomotor activity (Supplementary Fig. 6*A–D*).

Depletion of CUL4B From Adipose Tissues Led to Enhanced Adipocyte Differentiation

An increase in adipose tissue mass could result from hypertrophy, hyperplasia, or both. Hematoxylin-eosin staining of adipose tissues showed that adipocytes from HFD-fed AKO mice were smaller than WT adipocytes, especially in ingWAT (Fig. 3*A*). The diameters of subcutaneous adipocytes in WT mice measured 110 μm in average, whereas in AKO mice they measured 91 μm (Fig. 3*B*), indicating that hyperplasia may play a major role in adipose tissue expansion in AKO mice. Interestingly, adipocytes from NCD-fed AKO mice were also smaller than those from NCD-fed WT mice (Fig. 3*C* and *D*), suggesting that the lack of CUL4B in adipose tissues led to enhanced adipocyte differentiation under both NCD and HFD conditions, even though body weight gain and fat mass were comparable between two genotypes receiving NCD.

Adipocyte-Specific Deletion of *Cul4b* Protects From HFD-Induced Systemic Insulin Resistance

Obesity is correlated with glucose intolerance and insulin resistance. Therefore, we next assessed the effects of adipocyte-specific *Cul4b* deletion on glucose homeostasis and insulin sensitivity. Glucose tolerance, insulin sensitivity, and fasting insulin levels were comparable between WT and AKO mice that were eating a NCD (Fig. 4*A–C*). However, both glucose intolerance and insulin resistance induced by HFD were significantly attenuated in AKO mice when compared with WT mice (Fig. 4*D* and *E*), indicating that *Cul4b* deficiency could reduce HFD-induced insulin resistance. Consistent with the insulin tolerance test results, fasting insulin and free fatty acid levels were significantly lower in HFD-fed AKO mice (Fig. 4*F* and *G*), whereas the concentration of serum adiponectin was significantly higher than that in WT littermates (Fig. 4*H*). Collectively, these results suggest that adipocyte-specific *Cul4b* deficiency improved the overall metabolic phenotypes associated with HFD-induced obesity.

To further confirm the beneficial effect of CUL4B deficiency, we examined the effect of CUL4B deficiency on insulin action. As shown in Fig. 4*I* and *J*, insulin-stimulated phosphorylation of insulin receptor (p-IR; Tyr1162, 1163) and of Akt (p-Akt; Ser473) was increased in adipose tissue, and liver and skeletal muscle, of AKO mice, indicating that *Cul4b* deficiency in adipocytes can protect all three major insulin target tissues from HFD-induced insulin resistance. We also measured insulin-stimulated glucose uptake in primary adipocytes and confirmed the increased glucose transport in AKO mice versus WT mice (Fig. 4*K*). Together, these data demonstrated that the deletion of CUL4B in adipocytes can markedly increase systemic insulin sensitivity.

Reduced Adipose Tissue Inflammation in AKO Mice in Response to HFD Feeding

Previous studies have shown that obesity is associated with a chronic low-grade inflammation that facilitates the development of insulin resistance. Increased macrophage infiltration in adipose tissue is a hallmark of obesity-induced tissue inflammation (24,25). We performed immunostaining for the macrophage marker F4/80 and scored the crown-like structures. The numbers of crown-like structures were decreased in HFD-fed AKO mice when compared with those in WT mice (Fig. 5*A*). In addition, we analyzed SVFs from adipose tissues of HFD-fed WT and AKO mice by flow cytometry. $F4/80^+CD11b^+$ macrophages and $CD11c^+$ proinflammatory macrophages ($F4/80^+CD11b^+CD11c^+$) were significantly reduced in abundance in both epiWAT and ingWAT of AKO mice (Fig. 5*B* and *C*), suggesting that macrophage recruitment to adipose tissues was reduced by the lack of CUL4B. Consistent with these findings, quantitative RT-PCR analysis revealed that the expression of *Emr1* (F4/80) and

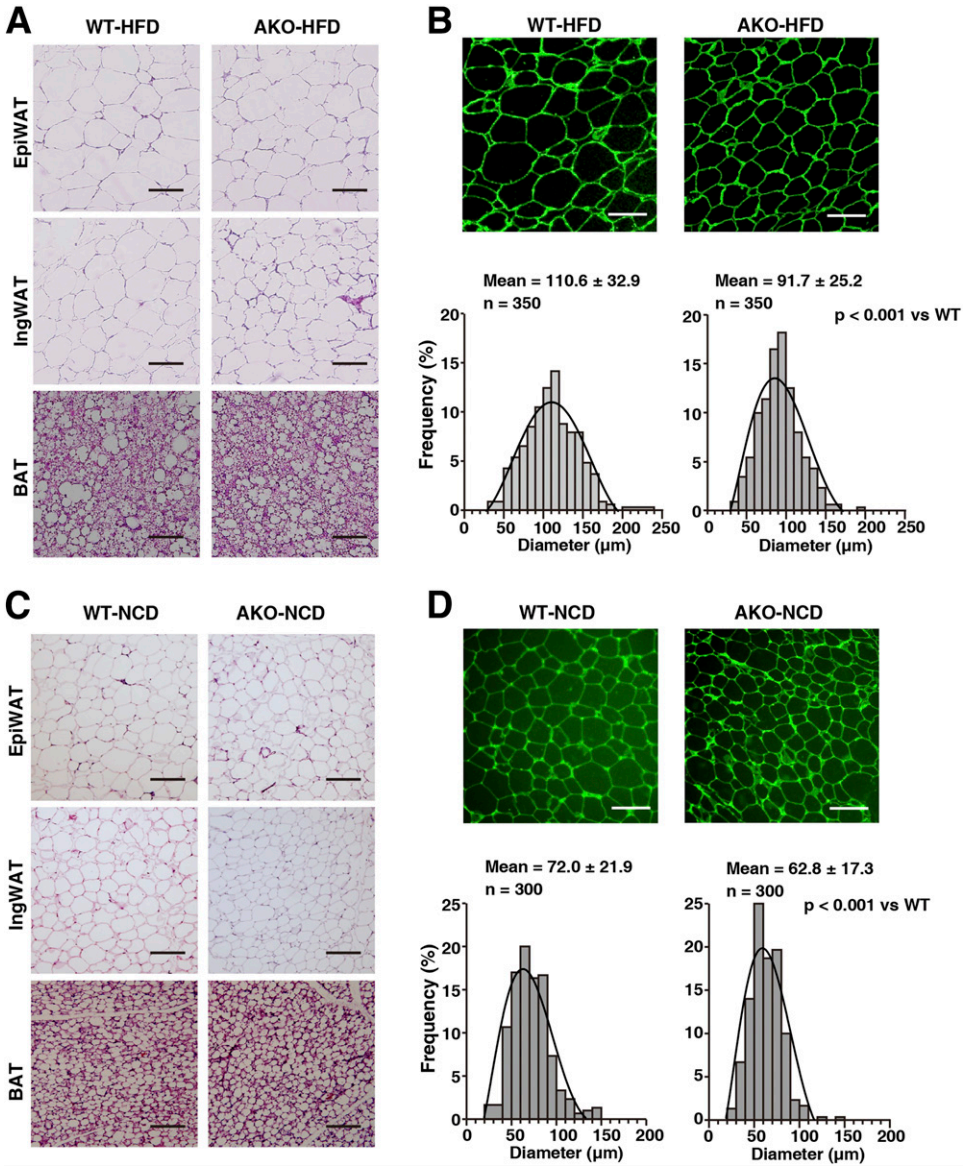

Figure 3—Increased adipogenesis in AKO mice. The 8-week-old male WT and AKO mice were fed an HFD or NCD for an additional 16 weeks. *A* and *C*: Representative hematoxylin-eosin–stained images of epiWAT, ingWAT, and BAT. *B* and *D*: Top, representative caveolin-stained images of ingWAT. Bottom, quantification of adipocyte diameter. A total of 300–350 cells, 50 cells/mouse, were measured (n = 6–7 for each group). Scale bars, 100 μm. The data are presented as the mean ± SEM. $P < 0.001$ for AKO vs. WT by Student t test.

genes marking M1 macrophage activation such as *Itgax* (CD11c) was downregulated in adipose tissue of AKO mice, whereas the expression of *Arg1* and *Ym-1*, indicators of anti-inflammatory macrophages, were upregulated (Fig. 5*D*). To determine whether these changes in mRNA expression in adipose tissues were related to systemic inflammation, we measured tumor necrosis factor-α (TNF-α), interleukin (IL)-6, IL-1β, MCP-1, and IL-10 levels in the blood. Although plasma levels of TNF-α, IL-6, IL-1β, and IL-10 were not significantly different between two genotypes, plasma levels of MCP-1 were significantly lower in AKO mice than in WT mice fed an HFD (Fig. 5*E*). Furthermore, we performed transwell chemotaxis assay by exposing macrophages to conditioned media prepared from *Cul4b*-deficient and WT adipocytes, respectively, and observed a reduced chemotaxis of macrophages conferred by media from *Cul4b*-deficient adipocytes (Fig. 5*F*), suggesting that alterations in chemokine secretion by AKO adipocytes might be responsible for the decreased macrophage chemotaxis. This result substantiated the notion of a reduced inflammatory response in *Cul4b*-deficient adipose tissues.

Enhanced Adipocyte Hyperplasia and Decreased HFD-Induced Adipose Inflammation Are Mediated by Upregulation of PPARγ

The fact that the deletion of CUL4B in adipose tissue phenocopied the beneficial effects of TZD treatment suggested that CUL4B might negatively regulate PPARγ

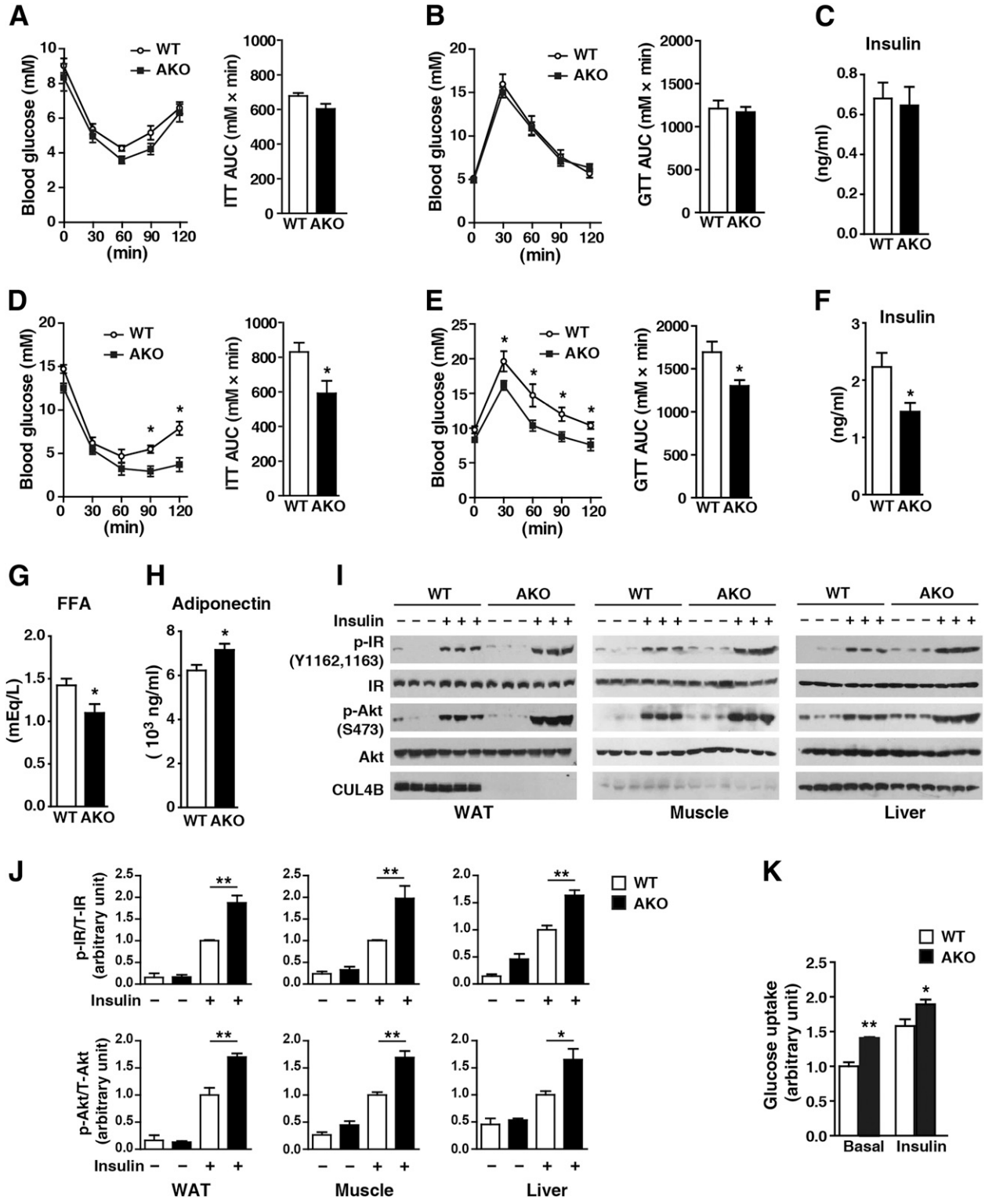

Figure 4—Improved insulin sensitivity in HFD-fed AKO mice. *A–C*: The 8-week-old male WT and AKO mice were grouped (n = 8 for each group) and fed with NCD for an additional 16 weeks. During the last week, insulin tolerance (*A*), glucose tolerance (*B*), and fast insulin levels (*C*) were measured. The area under the curve (AUC) was quantified. *D–H*: The 8-week-old male WT and AKO mice were fed an HFD for 16 weeks (n = 7 for each group). *D*: Insulin tolerance tests (ITTs). *E*: Glucose tolerance tests (GTTs). Fasting plasma concentrations of insulin (*F*), free fatty acid (FFA; *G*), and adiponectin (*H*). *I* and *J*: Basal and insulin-stimulated p-IR (Tyr1162, Tyr1163) and p-Akt (Ser473) in WAT, muscle, and liver. The HFD-fed mice were injected intraperitoneally with insulin (1 unit/kg). *I*: Tissues were excised 10 min after injection for IB analyses. *J*: The p-IR/total IR and p-Akt/total Akt ratios were calculated. *K*: Basal and insulin-stimulated ^{3}H-2-deoxyglucose uptake in primary adipocytes. 2-Deoxyglucose uptake was measured over 5 min after stimulation ± insulin for 30 min. All the data are presented as the mean ± SEM. $^*P < 0.05$, $^{**}P < 0.01$ for AKO vs. WT by Student t test.

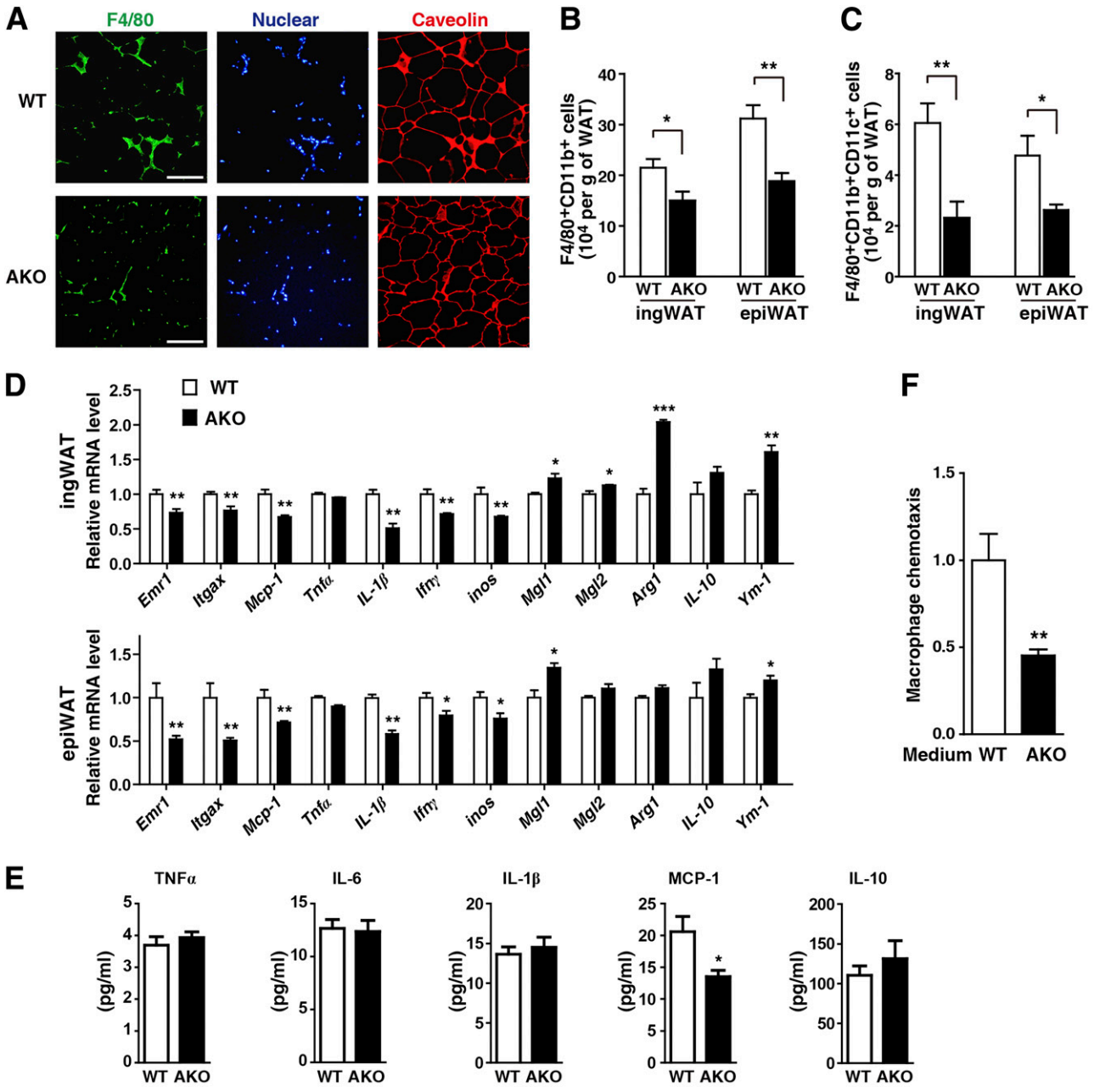

Figure 5—Decreased adipose tissue inflammation in HFD-fed AKO mice. The 8-week-old male WT and AKO mice were fed an HFD for 16 weeks (n = 5 for each group). *A*: Representative F4/80 and caveolin-immunostained images of ingWAT. Scale bars, 100 μm. *B* and *C*: The numbers of macrophages per gram of ingWAT or epiWAT. FACS analysis of F4/80$^+$CD11b$^+$ (*B*) and F4/80$^+$CD11b$^+$CD11c$^+$ cells (*C*) in SVFs. *D*: Relative mRNA levels of inflammatory and anti-inflammatory cytokines in ingWAT or epiWAT. *E*: The levels of circulating inflammatory cytokines in WT and AKO mice. *F*: Effect of conditioned medium from WT and AKO primary adipocytes on macrophage chemotaxis. Values are expressed as the mean ± SEM. *P < 0.05, **P < 0.01, ***P < 0.001 for AKO vs. WT by Student t test.

level and activity. Therefore, we next examined the effect of CUL4B ablation on the level of PPARγ. As shown in Fig. 6*A* and Supplementary Fig. 7, the levels of PPARγ protein were significantly increased in WATs of both NCD- and HFD-fed AKO mice but were only slightly increased in BAT. However, the transcript level of *Pparγ* was unchanged (Fig. 6*B*), suggesting that *Cul4b* deficiency does not affect *Pparγ* transcription. Consistent with the increased level of PPARγ in the absence of CUL4B in vivo, overexpression of CUL4B, but not of mutant CUL4B (Cullin domain deleted [CUL4BΔCullin]), in HEK293 cells resulted in a reduction of PPARγ protein (Fig. 6*C*). Importantly, the reduction of PPARγ caused by the overexpression of CUL4B was efficiently blocked by the administration of MG132 (a proteasome inhibitor) but not of chloroquine (an inhibitor of lysosomal proteolysis) (Fig. 6*D*), implying that CUL4B may downregulate PPARγ via a proteasome-dependent degradation mechanism. To further strengthen

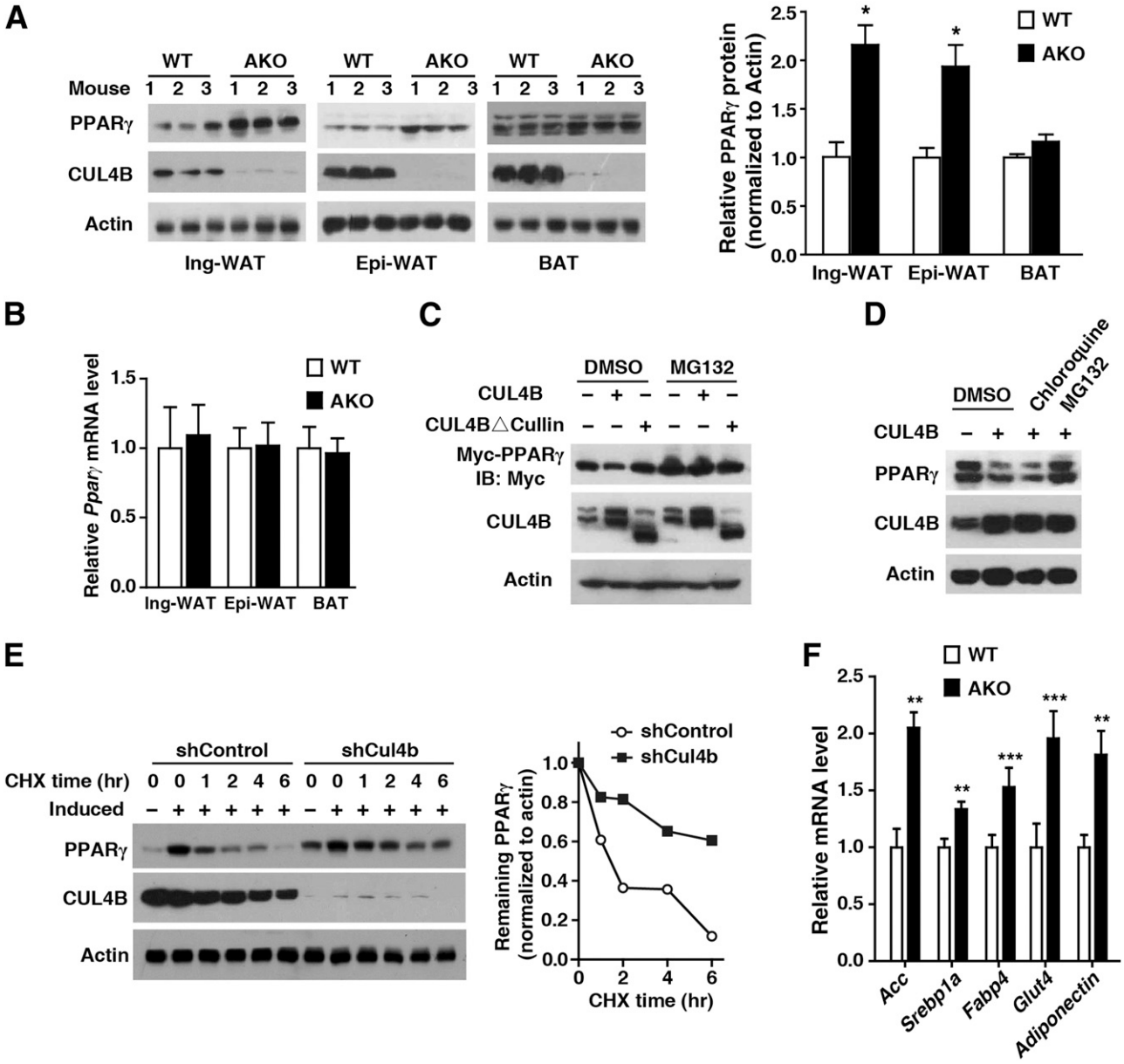

Figure 6—Depletion of CUL4B increases the stability of PPARγ protein. *A*: The PPARγ protein levels in adipose depots of mice fed with HFD for 16 weeks ($n = 3$ per group). The band intensity was measured and normalized to loading control. The expression was presented as the fold changes relative to WT. *B*: The *Pparγ* mRNA levels in mice from *A*. *C*: HEK293 cells were transfected with the plasmids expressing Myc-PPARγ and CUL4B or CUL4BΔCullin. After 24 h, the cells were treated with MG132; cell lysates were then harvested and analyzed by Western blotting using the indicated antibodies. *D*: 3T3-L1 cells stably expressing CUL4B were constructed using a lentivirus expressing CUL4B (empty vector as control). The cells were treated with chloroquine or MG132 for 2 h and analyzed by Western blotting using the indicated antibodies. *E*: 3T3-L1 cells stably expressing shRNA for *Cul4b* (shCul4b) or nontargeting control shRNA (shControl) were differentiated for 2 days, followed by incubating with CHX for various times and then Western blotting analysis. Expression is represented as the percentage of PPARγ protein remaining relative to time zero. *F*: The mRNA levels of adipogenic/lipogenic genes in ingWAT of mice in *A*. All data are shown as the mean ± SEM. $^*P < 0.05$, $^{**}P < 0.01$, $^{***}P < 0.001$ determined by Student *t* test.

this notion, we measured PPARγ protein half-life in the CUL4B knockdown cells. After translation inhibition by cycloheximide (CHX), the levels of PPARγ gradually dropped to a very low level within 6 h. Remarkably, the knockdown of CUL4B resulted in a much slower PPARγ decay (Fig. 6*E*). These results suggested that CUL4B decreases the stability of PPARγ protein.

PPARγ transcriptional activity plays a pivotal role in adipogenesis. We next determined whether the increased stability of PPARγ in AKO mice could be translated into an enhanced transactivation activity. As shown in Fig. 6*F*, depletion of CUL4B resulted in significantly increased expression of PPARγ-regulated genes, including *Acc*, *Srebp1a*, *Fabp4*, *Glut4*, and *Adiponectin*, in adipose tissue of AKO mice.

These results suggest that increased PPARγ activity might be responsible for improved adipocyte function and enhanced adipogenesis in AKO mice. Importantly, PPARγ depletion by RNA interference (RNAi) or inhibition by the small molecular inhibitor GW9662 (26) efficiently blunted the glucose uptake in *Cul4b* knockdown 3T3-L1 cells (Fig. 7*A* and *B*). As shown in Fig. 7*C* and *D*, GW9662 also efficiently blocked the increased weight gain and ingWAT accumulation in HFD-fed AKO mice. Notably, GW9662 negated the upregulation of PPARγ-regulated genes caused by CUL4B depletion (Fig. 7*E*). Histological analysis showed that the reduction in adipocyte size caused by CUL4B deletion was attenuated by GW9662 administration (Supplementary Fig. 8). Furthermore, the administration of GW9662 equaled the expression levels of proinflammatory genes and anti-inflammatory genes in HFD-fed AKO and WT mice (Fig. 7*F* and *G*). Together, these data indicate that enhanced adipocyte hyperplasia and decreased HFD-induced adipose tissue inflammation in AKO mice are mediated by increased PPARγ activity.

CRL4B Functions as an E3 Ligase for PPARγ

CUL4B functions as a scaffold for the multisubunit E3 ligase complex CRL4B (27,28). We next tested whether PPARγ is a direct substrate of CRL4B. We first characterized the roles of the different domains of CUL4B in PPARγ degradation. As shown in Fig. 8*A*, when expressed, only the full-length CUL4B resulted in a PPARγ reduction, whereas nuclear localization signal–deleted CUL4B, DDB1-interacting domain–deleted CUL4B, or CUL4BΔCullin did not, suggesting that the DDB1-interacting domain and Cullin domain are required for the negative regulation of PPARγ. In addition, the ectopic expression of CUL4A did not appear to affect the level of PPARγ. Consistently, the knockdown of DDB1, but not of CUL4A, resulted in a significant increase in the half-life of PPARγ (Fig. 8*B*). These results implied that CRL4B complex might function as an E3 ligase for PPARγ. We then determined the possible physical association between CRL4B complex and PPARγ. Indeed, when PPARγ was immunoprecipitated from 3T3-L1 cells, a substantial amount of CUL4B and DDB1 was brought down as well, whereas CUL4A was not coimmunoprecipitated (Fig. 8*C*). Consistently, PPARγ was coimmunoprecipitated with antibodies against CUL4B in both ingWAT and epiWAT (Fig. 8*D*). In addition, treatment with MG132 increased the amount of PPARγ that was pulled down by CUL4B (Fig. 8*E*). An in vitro ubiquitination assay showed that although the full-length CUL4B significantly increased the amount of polyubiquitinated PPARγ, the deletion of Cullin domain abrogated such enzymatic activity, indicating that PPARγ was directly degraded through the CRL4B-mediated Ub proteasome system (Fig. 8*F*). When a plasmid-encoding, Myc-labeled full-length PPARγ was cotransfected into HEK293 cells with HA-tagged Ub, a substantial amount of polyubiquitinated PPARγ was detected, whereas the knockdown of CUL4B resulted in a reduction of polyubiquitinated PPARγ (Fig. 8*G*). Consistently, polyubiquitinated PPARγ was also reduced in CUL4B knockdown 3T3-L1 cells (Fig. 8*H*), whereas the overexpression of CUL4B in 3T3-L1 cells significantly increased the polyubiquitination of PPARγ (Fig. 8*I*). Together, these results support that CRL4B functions as an E3 ligase for PPARγ.

DISCUSSION

CUL4B participates in the regulation of a broad spectrum of biological processes. In the current study, we provided several lines of evidence that CUL4B functions as a negative regulator of adipogenesis. First, CUL4B expression was downregulated during adipocyte differentiation in obese mice and was inversely correlated with BMI. Second, knockdown of CUL4B in 3T1-L1 cells led to increased adipocyte differentiation, whereas the overexpression of CUL4B had the opposite effect. Third, most importantly, the deletion of CUL4B in adipose tissues greatly facilitated adipogenesis. When challenged with HFD, AKO mice exhibited increased body weight gain and fat mass. Mechanistically, we demonstrated that the negative regulation of adipogenesis by CUL4B is mediated by the polyubiquitination of PPARγ, a master regulator of adipogenesis and insulin sensitivity. In particular, the treatment with PPARγ inhibitor GW9662 in HFD-fed AKO mice could efficiently block the increased adipogenesis and decreased adipose inflammatory response to obesity. Together, our findings establish CUL4B as a novel regulator of PPARγ-mediated adipogenesis.

The phenotypes caused by *Cul4b* deficiency are reminiscent of those by a constitutive PPARγ activation. For example, PPARγ agonist TZDs generally increase subcutaneous fat mass. Correspondingly, *Cul4b* deficiency resulted in a pronounced accumulation of fat in the subcutaneous depot, which favors metabolic health. Additionally, both TZD treatment and *Cul4b* deficiency promote adipocyte hyperplasia. Furthermore, despite increased obesity, the HFD-fed AKO mice showed improved metabolic phenotypes, including increased insulin sensitivity and glucose tolerance, increased the expression of adiponectin, and reduced the level of free fatty acid. Abundant evidence implicates adipose inflammation in the pathogenesis of insulin resistance triggered by obesity. We observed that improved insulin sensitivity in HFD-fed AKO mice was accompanied by decreased adipose inflammation, as demonstrated by decreased adipose tissue macrophage accumulation, increased M2/M1 ratio, decreased expression of proinflammatory genes, and increased expression in anti-inflammatory genes. The decreased MCP-1 production in AKO mice may have accounted for the decreased adipose tissue macrophage accumulation and reduced inflammation. Thus, the adipocyte-specific deletion of *Cul4b* and constitutive PPARγ activation appear to share the same spectrum of phenotypes.

Given its critical roles in adipogenesis and metabolic homeostasis, PPARγ function is expected to be tightly regulated. Using RNAi-based screening, Ub ligase Siah2 was identified to facilitate ubiquitination and degradation of PPARγ in mature 3T3-L1 adipocytes, probably by

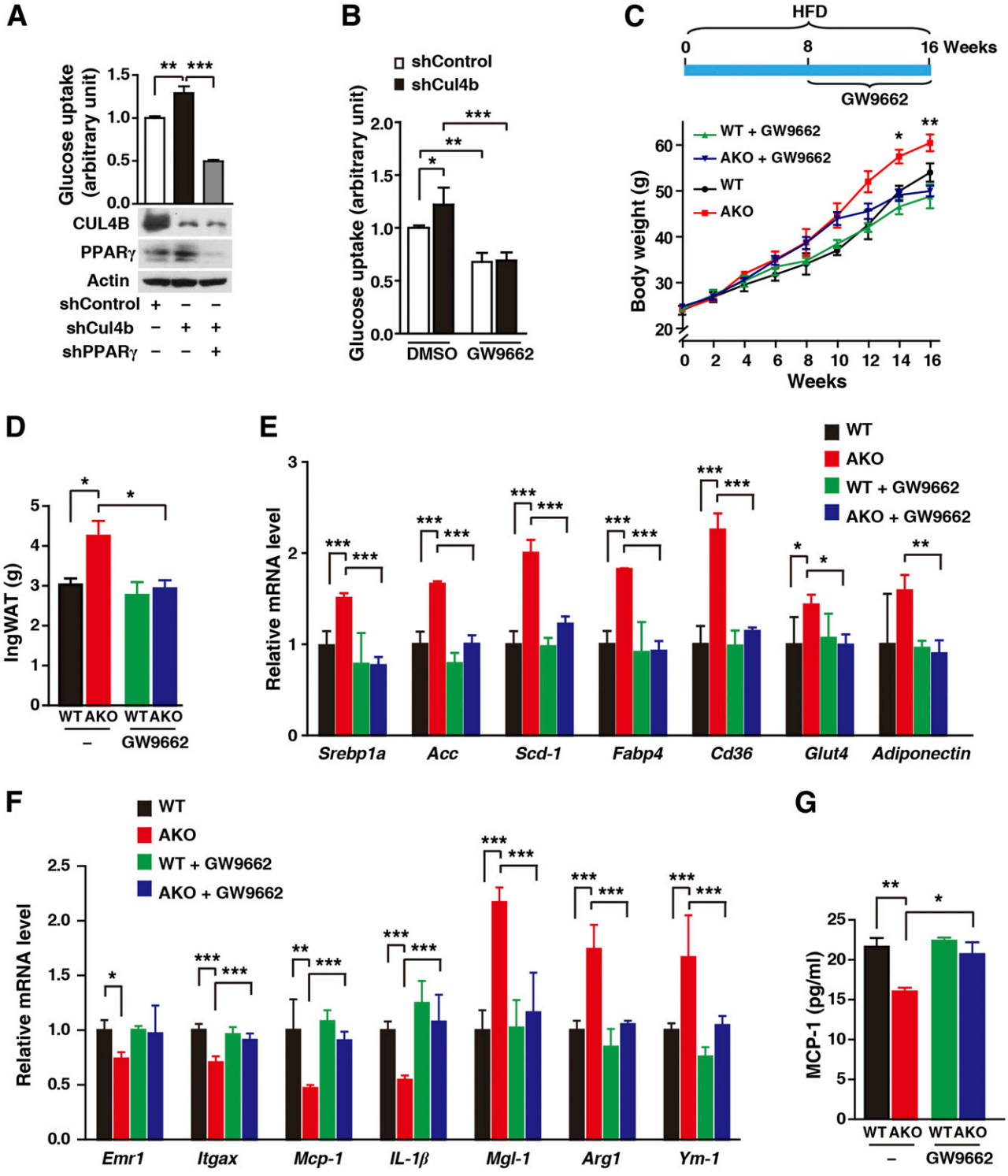

Figure 7—PPARγ inhibition blocks increased adipogenesis and decreased adipose inflammation caused by the depletion of CUL4B. *A*: Quantification of radiolabeled ^{3}H-2-deoxyglucose uptake in 3T3-L1 cells in which *Cul4b* or both *Cul4b* and *Pparγ* were knocked down by RNAi. *B*: Quantification of radiolabeled ^{3}H-2-deoxyglucose uptake in *Cul4b* knockdown 3T3-L1 cells treated with or without GW9662. *C–G*: The 8-week-old WT and AKO mice were fed with HFD for 16 weeks (n = 5 for each group). During the 8–16 weeks, the mice were administered GW9662. The top panel in *C* shows the scheme of the treatment model. Body weight (*C*) and ingWAT weight (*D*) are shown in the indicated groups. $^{*}P < 0.05$, $^{**}P < 0.01$ for AKO vs. AKO+GW9662 (*C*). *E*: The relative mRNA levels of adipogenic/lipogenic genes in ingWAT. *F*: Relative mRNA levels of inflammatory and anti-inflammatory cytokines in ingWAT. *G*: Plasma protein levels of MCP-1. All data are shown as the mean ± SEM. $^{*}P < 0.05$, $^{**}P < 0.01$, $^{***}P < 0.001$ determined by ANOVA.

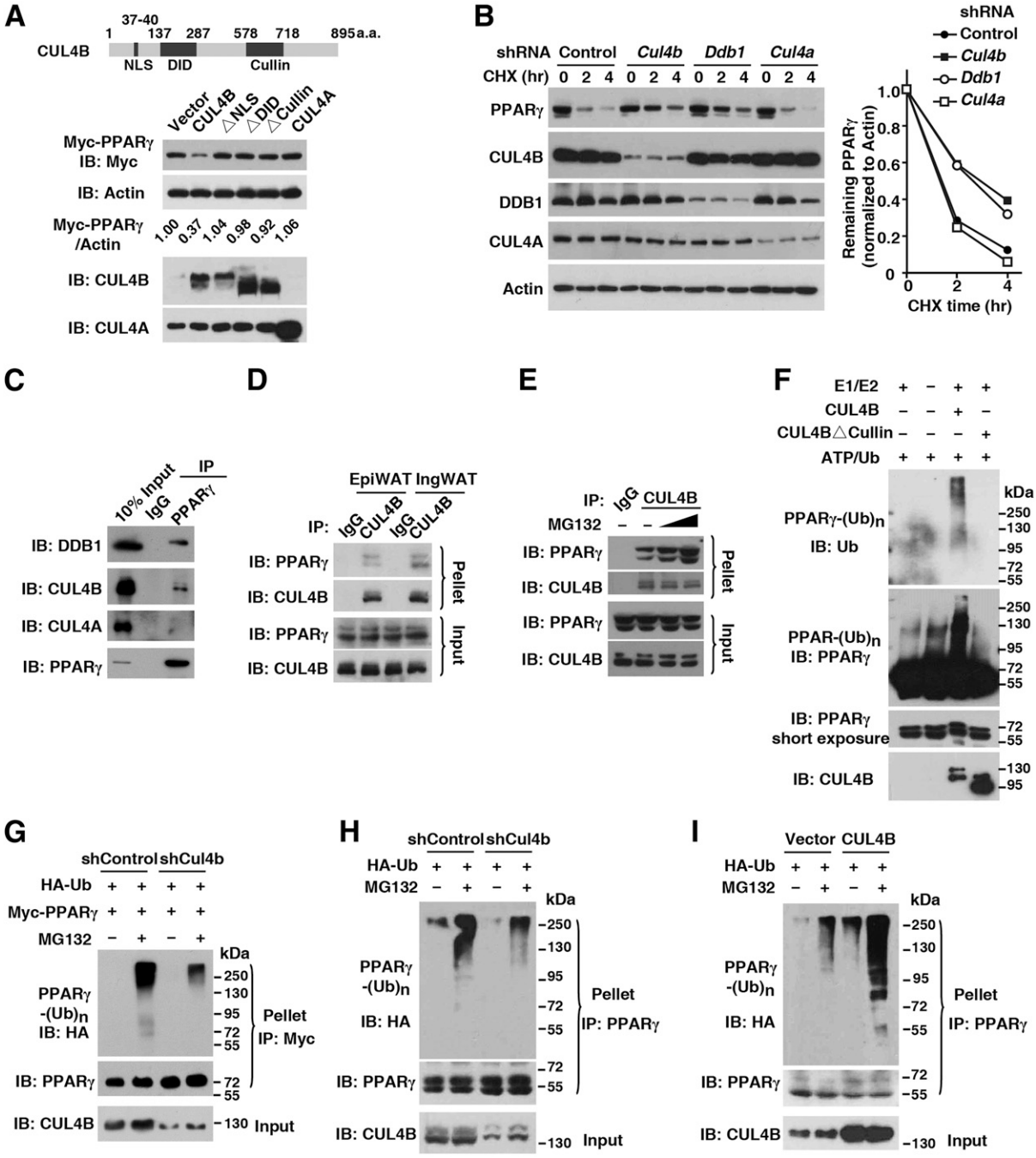

Figure 8—CRL4B complex catalyzes ubiquitination of PPARγ. *A*: The top panel shows the schematic of the CUL4B domains. The *CUL4B* knockdown HEK293 cells were transfected with the plasmids encoding Myc-PPARγ and CUL4B or CUL4B with deletions or CUL4A, and 24 h later the cell lysates were subjected to IB. The band intensity given underneath the gel image was presented as the fold change compared with cells transfected with empty vector. *B*: 3T3-L1 cells stably expressing shRNA targeting the indicated genes were induced to undergo differentiation for 2 days, followed by incubating with CHX for various times. Then the cell lysates were subjected to IB. The percentage of PPARγ protein remaining relative to 0 h was calculated. *C*: 3T3-L1 cells were subjected to immunoprecipitation (IP) with anti-PPARγ antibody and the resulting precipitates as well as a portion (10% of the input) of the cell lysates were immunoblotted with the indicated antibodies. *D*: The epiWAT and ingWAT from 12-week-old C57BL/6 male mice were subjected to IP with anti-CUL4B antibody. *E*: 3T3-L1 cells were incubated with DMSO or MG132 (3 and 10 μmol/L) for 2 h, then the cells were harvested and whole cell lysates were immunoprecipitated using IgG or anti-CUL4B antibody. *F*: Ubiquitination of PPARγ by CRL4B complex in vitro. Purified recombinant His-PPARγ was incubated with E1, E2, Ub, and ATP in the absence and presence of CRL4B complex (WT or Cullin deletion) as indicated. Ubiquitination of PPARγ was analyzed by Western blotting using anti-Ub or anti-PPARγ antibodies. *G*: CUL4B-dependent ubiquitination of PPARγ. HEK293 cells stably expressing control shRNA or shRNA targeting *Cul4b* were transfected with HA-Ub and Myc-PPARγ and treated with MG132 (10 μmol/L) or DMSO. Myc-PPARγ was pulled down using anti-Myc beads and detected using anti-PPARγ or anti-HA antibodies. *H* and *I*: 3T3-L1 cells stably expressing *Cul4b* shRNA (*H*) or CUL4B (*I*) were transfected with HA-Ub and treated with MG132 (10 μmol/L) or DMSO. PPARγ was pulled down using anti-PPARγ beads and detected using anti-PPARγ or anti-HA antibodies.

targeting a nuclear receptor corepressor, NCoR (29,30). More recently, Makorin Ring Finger Protein 1 was identified to be an E3 ligase that directly targets PPARγ for proteasomal degradation in a ligand-dependent manner (14). Strikingly, Ub E3 ligase tripartite motif protein 23 was shown to stabilize PPARγ via atypical poly-Ub conjugation, including M1- and K27-linked Ub chains to PPARγ (31). Thus, different E3 ligases may have opposite effects on the stability of PPARγ. We here demonstrated CUL4B-based Ub ligase to be a novel E3 ligase that targets PPARγ for polyubiquitination and subsequent degradation.

Our observation that a lack of CUL4B in adipocytes could cause enhanced systemic insulin sensitivity is consistent with the phenotype observed in adipocyte-specific *NCoR* knockout mice (11). The dominant function of adipocyte NCoR is to transrepress PPARγ and facilitate CDK5-mediated PPARγ phosphorylation at serine 273, thereby inhibiting PPARγ activity. Importantly, both studies suggest that unleashing PPARγ in adipose tissue alone is sufficient for producing the systemic effects seen with in vivo TZD treatment.

In summary, CUL4B functions as a negative regulator of adipogenesis via targeting PPARγ for proteasomal degradation. Lack of CUL4B in adipocytes improves adipose function and protects against glucose intolerance and insulin resistance in HFD-induced obesity. These features phenocopy the beneficial effects of TZD treatment. Therefore, CUL4B is a potential target for ameliorating metabolic abnormalities. Future studies need to determine how CUL4B is downregulated during adipogenesis and which CUL4-DDB1–associated factor is used for CUL4B to recognize PPARγ.

Funding. This work was supported by State Program of National Natural Science Foundation of China for Innovative Research Group (grant 81321061 to C.S. and Y.G.), the National Natural Science Foundation of China (grants 81330050 and 81571523 to Y.G.; grant 81400841 to P.L.), the Natural Science Foundation of Shandong Province (grants ZR2015HZ002 to Y.G. and ZR2014HQ055 to P.L.), the China Postdoctoral Science Foundation (grants 2014M561918 and 2015T80711 to P.L.), and the Young Scholars Program of Shandong University (to P.L.).

Duality of Interest. No potential conflicts of interest relevant to this article were reported.

Author Contributions. P.L. designed the studies, performed experiments, and wrote the manuscript. Y.S., W.Z., L.Q., and S.H. performed experiments. B.J. and H.D. provided mice, reagents, and advice. C.S. contributed intellectually and wrote the manuscript. Y.G. designed the studies, supervised research, and wrote the manuscript. Y.G. is the guarantor of this work and, as such, had full access to all the data in the study and takes responsibility for the integrity of the data and the accuracy of the data analysis.

References

1. He W, Barak Y, Hevener A, et al. Adipose-specific peroxisome proliferator-activated receptor gamma knockout causes insulin resistance in fat and liver but not in muscle. Proc Natl Acad Sci U S A 2003;100:15712–15717

2. Imai T, Takakuwa R, Marchand S, et al. Peroxisome proliferator-activated receptor gamma is required in mature white and brown adipocytes for their survival in the mouse. Proc Natl Acad Sci U S A 2004;101:4543–4547

3. Sugii S, Olson P, Sears DD, et al. PPARgamma activation in adipocytes is sufficient for systemic insulin sensitization. Proc Natl Acad Sci U S A 2009;106:22504–22509

4. Harris PK, Kletzien RF. Localization of a pioglitazone response element in the adipocyte fatty acid-binding protein gene. Mol Pharmacol 1994;45:439–445

5. Lehmann JM, Moore LB, Smith-Oliver TA, Wilkison WO, Willson TM, Kliewer SA. An antidiabetic thiazolidinedione is a high affinity ligand for peroxisome proliferator-activated receptor gamma (PPAR gamma). J Biol Chem 1995;270:12953–12956

6. Nesto RW, Bell D, Bonow RO, et al. Thiazolidinedione use, fluid retention, and congestive heart failure: a consensus statement from the American Heart Association and American Diabetes Association. Diabetes Care 2004;27:256–263

7. Soccio RE, Chen ER, Lazar MA. Thiazolidinediones and the promise of insulin sensitization in type 2 diabetes. Cell Metab 2014;20:573–591

8. Eeckhoute J, Oger F, Staels B, Lefebvre P. Coordinated regulation of ppargamma expression and activity through control of chromatin structure in adipogenesis and obesity. PPAR Res 2012;2012:164140

9. Wadosky KM, Willis MS. The story so far: post-translational regulation of peroxisome proliferator-activated receptors by ubiquitination and SUMOylation. Am J Physiol Heart Circ Physiol 2012;302:H515–H526

10. Choi JH, Banks AS, Estall JL, et al. Anti-diabetic drugs inhibit obesity-linked phosphorylation of PPARgamma by Cdk5. Nature 2010;466:451–456

11. Li P, Fan W, Xu J, et al. Adipocyte NCoR knockout decreases PPARγ phosphorylation and enhances PPARγ activity and insulin sensitivity. Cell 2011;147:815–826

12. Banks AS, McAllister FE, Camporez JP, et al. An ERK/Cdk5 axis controls the diabetogenic actions of PPARγ. Nature 2015;517:391–395

13. Dutchak PA, Katafuchi T, Bookout AL, et al. Fibroblast growth factor-21 regulates PPARγ activity and the antidiabetic actions of thiazolidinediones. Cell 2012;148:556–567

14. Kim JH, Park KW, Lee EW, et al. Suppression of PPARγ through MKRN1-mediated ubiquitination and degradation prevents adipocyte differentiation. Cell Death Differ 2014;21:594–603

15. Hauser S, Adelmant G, Sarraf P, Wright HM, Mueller E, Spiegelman BM. Degradation of the peroxisome proliferator-activated receptor gamma is linked to ligand-dependent activation. J Biol Chem 2000;275:18527–18533

16. Floyd ZE, Stephens JM. Interferon-gamma-mediated activation and ubiquitin-proteasome-dependent degradation of PPARgamma in adipocytes. J Biol Chem 2002;277:4062–4068

17. Jackson S, Xiong Y. CRL4s: the CUL4-RING E3 ubiquitin ligases. Trends Biochem Sci 2009;34:562–570

18. Hu H, Yang Y, Ji Q, et al. CRL4B catalyzes H2AK119 monoubiquitination and coordinates with PRC2 to promote tumorigenesis. Cancer Cell 2012;22:781–795

19. He F, Lu D, Jiang B, Wang Y, Liu Q, Liu Q, Shao C, Li X, Gong Y. X-linked intellectual disability gene CUL4B targets Jab1/CSN5 for degradation and regulates bone morphogenetic protein signaling. Biochim Biophys Acta 2013;1832:595–605

20. Zou Y, Liu Q, Chen B, et al. Mutation in CUL4B, which encodes a member of cullin-RING ubiquitin ligase complex, causes X-linked mental retardation. Am J Hum Genet 2007;80:561–566

21. Tarpey PS, Raymond FL, O'Meara S, et al. Mutations in CUL4B, which encodes a ubiquitin E3 ligase subunit, cause an X-linked mental retardation syndrome associated with aggressive outbursts, seizures, relative macrocephaly, central obesity, hypogonadism, pes cavus, and tremor. Am J Hum Genet 2007;80:345–352

22. Jiang B, Zhao W, Yuan J, et al. Lack of Cul4b, an E3 ubiquitin ligase component, leads to embryonic lethality and abnormal placental development. PLoS One 2012;7:e37070

23. Skrzypski M, T Le T, Kaczmarek P, et al. Orexin A stimulates glucose uptake, lipid accumulation and adiponectin secretion from 3T3-L1 adipocytes and isolated primary rat adipocytes. Diabetologia 2011;54:1841–1852

24. McNelis JC, Olefsky JM. Macrophages, immunity, and metabolic disease. Immunity 2014;41:36–48
25. Ouchi N, Parker JL, Lugus JJ, Walsh K. Adipokines in inflammation and metabolic disease. Nat Rev Immunol 2011;11:85–97
26. Leesnitzer LM, Parks DJ, Bledsoe RK, et al. Functional consequences of cysteine modification in the ligand binding sites of peroxisome proliferator activated receptors by GW9662. Biochemistry 2002;41:6640–6650
27. Petroski MD, Deshaies RJ. Function and regulation of cullin-RING ubiquitin ligases. Nat Rev Mol Cell Biol 2005;6:9–20
28. Hannah J, Zhou P. Distinct and overlapping functions of the cullin E3 ligase scaffolding proteins CUL4A and CUL4B. Gene 2015;573:33–45
29. Kilroy G, Kirk-Ballard H, Carter LE, Floyd ZE. The ubiquitin ligase Siah2 regulates PPARγ activity in adipocytes. Endocrinology 2012;153:1206–1218
30. Kilroy G, Carter LE, Newman S, et al. The ubiquitin ligase Siah2 regulates obesity-induced adipose tissue inflammation. Obesity (Silver Spring) 2015;23:2223–2232
31. Watanabe M, Takahashi H, Saeki Y, et al. The E3 ubiquitin ligase TRIM23 regulates adipocyte differentiation via stabilization of the adipogenic activator PPARγ. eLife 2015;4:e05615